Inorg. Chem. **2008**, *47*, 508–514

Structural Phase Stability Studies on $MBeH_3$ (M = Li, Na, K, Rb, Cs) from Density Functional Calculations

P. Vajeeston,* P. Ravindran, and H. Fjellvåg

Department of Chemistry, Center for Materials Sciences and Nanotechnology, University of Oslo, Box 1033 Blindern, N-0315 Oslo, Norway

Received August 9, 2007

Density functional theory calculations within the generalized-gradient approximation are used to establish the ground-state structure, equilibrium structural parameters, and electronic structure for $MBeH_3$ phases. From the 24 structural arrangements used as inputs for structural optimization calculations, the ground-state crystal structures of $MBeH_3$ phases have been predicted. At ambient conditions, $LiBeH_3$ and $NaBeH_3$ crystallize with perovskite-related orthorhombic and cubic structures, respectively. The remaining phases $KBeH_3$, $RbBeH_3$, and $CsBeH_3$ crystalize in a monoclinic structure. In the predicted phases one can store up to 15.93 wt % of hydrogen. The formation energy for the $MBeH_3$ phases have been investigated along different reaction pathways. The electronic structures reveal that all these phases are insulators with estimated band gaps varying between 1.79 and 3.44 eV.

I. Introduction

The crystal structure, shape, size, and surface composition of materials are major factors that control the hydrogen absorption properties for energy storage applications. To act as an efficient energy carrier, hydrogen should be absorbed and desorbed in materials easily and in high quantities. Alkali- and alkaline-earth-based complex hydrides are expected to have potential as viable modes for storing hydrogen at moderate temperatures and pressures.[1−7] These hydrides (e.g., $LiAlH_4$, $NaAlH_4$, etc.)[1−7] have higher hydrogen storage capacity at moderate temperatures than conventional hydride systems based on intermetallic compounds. The disadvantages for the use of these materials for practical applications are the lack of reversibility and poor kinetics. Recent experimental findings have shown that the decomposition temperature for certain complex hydrides can be modified by introduction of additives[3,4] and/or reduction of particle size.[8−11] This has opened up for research activity on identification of appropriate admixtures for known or hitherto unexplored hydrides. As proposed in our earlier communications,[12−14] it should be possible to form several series of hydrides with alkali and alkaline earth metals in combination with Group III elements of the Periodic Table. In our recent publication we have solved the crystal structure of the entire $MMgH_3$ (M = Li, Na, K, Rb, Cs) series,[15] where the crystal structure and equilibrium structural parameters for experimentally known phases have been reproduced and the structure of $LiMgH_3$ has been predicted. In the $MBeH_3$ phases one can store up to 15.93 wt % of hydrogen (e.g $LiBeH_3$). However, Be is an extremely toxic material, and special precautions are employed in its handling. Therefore, the structure of most of these phases is not yet established experimentally. In order to fill this gap, in this work we are reporting the electronic and crystal structures of all the

* To whom correspondence should be addressed. E-mail: ponniahv@kjemi.uio.no. URL: http://folk.uio.no/ponniahv.

(1) Block, J.; Gray, A. P. *Inorg. Chem.* **1965**, *304*, 4.
(2) Dilts, J. A.; Ashby, E. C. *Inorg. Chem.* **1972**, *11*, 1230. Bastide, J. P.; Monnetot, B.; Letoffe, J. M.; Claudy, P. Mater. *Res. Bull.* **1985**, *20*, 997.
(3) Bogdanovic, B.; Schwickardi, M. *J. Alloys Compd.* **1997**, *253*-254, 1.
(4) Bogdanovic, B.; Brand, R. A.; Marjanovic, A.; Schwikardi, M.; Tölle, J. *J. Alloys Compd.* **2000**, *302*, 36.
(5) Brinks, H. W.; Hauback, B. C.; Norby, P.; Fjellvåg, H. *J. Alloys Compd.* **2003**, *315*, 222.
(6) Jensen, C. M.; Gross, K. *J. Appl. Phys. A* **2001**, *72*, 213.
(7) Morioka, H.; Kakizaki, K.; Chung, S. C.; Yamada, A. *J. Alloys Compd.* **2003**, *353*, 310.
(8) Orimo, S.; Fujii, H.; Ikeda, K. *Acta Mater.* **1997**, *45*, 331.
(9) Zaluska, A.; Zaluski, L.; Ström-Olsen, J. O. *J. Alloys Compd.* **1999**, *288*, 217.
(10) Huot, J.; Liang, G.; Schultz, R. *Appl. Phys. A: Mater. Sci. Process.* **2001**, *72*, 187.
(11) Huot, J.; Pelletier, J. F.; Lurio, L. B.; Sutton, M.; Schulz, R. *J. Alloys Compd.* **2003**, *348*, 319.
(12) Vajeeston, P.; Ravindran, P.; Vidya, R.; Fjellvåg, H.; Kjekshus, A. *Cryst. Growth Des.* **2004**, *4*, 471.
(13) Vajeeston, P. *Theoretical Modeling of Hydrides*; ISSN 1501-7710, 2004.
(14) Vajeeston, P.; Ravindran, P.; Kjekshus, A.; Fjellvåg, H. *Appl. Phys. Lett.* **2006**, *89*, 071906.
(15) Vajeeston, P.; Ravindran, P.; Fjellvåg, H.; Kjekshus, A. *J. Alloys Compd.* **2006**, in press.

10.1021/ic7015897 CCC: $40.75
Published on Web 12/19/2007

$MBeH_3$ phases as derived from density functional theoretical calculations.

Computational Details. It is well known that the generalized-gradient approximation (GGA)[16] generally gives better equilibrium structural parameters and energetics of different phases, and hence, we have used GGA for all the present calculations. The structures are fully relaxed for all volumes considered using force and stress minimization. The projected-augmented-wave (PAW)[17] implementation of the Vienna ab initio simulation package (VASP)[18] was used for the total-energy calculations to establish phase stability and transition pressures. In order to avoid ambiguities regarding the free-energy results, same-energy cutoff and a similar **k**-grid density for convergence were always used. In all calculations 500 **k** points in the whole Brillouin zone were used for α-BeH_2 and a similar density of **k** points was used for all structural arrangements. A criterion of 0.01 meV $atom^{-1}$ was placed on the self-consistent convergence of the total energy, and all calculations used a plane-wave cutoff of 500 eV. The formation energies (ΔE) have been calculated according to the following reaction equations:

$$MH + BeH_2 \rightarrow MBeH_3 \quad (1)$$

$$M + BeH_2 + \frac{1}{2}H_2 \rightarrow MBeH_3 \quad (2)$$

$$MH + Be + H_2 \rightarrow MBeH_3 \quad (3)$$

$$M + Be + \frac{3}{2}H_2 \rightarrow MBeH_3 \quad (4)$$

The total energies of M, MH, and α-BeH_2 have been computed for the ground-state structures, viz. in space group $Im\bar{3}m$ for M, $Fm\bar{3}m$ for MH, and the previously reported[19] *Ibam* for α-BeH_2, all with full geometry optimization. To gauge the bond strength, we have used crystal orbital Hamilton population COHP analysis, as is implemented in the TBLMTO-47 package,[20] since this functionality is not yet implemented in VASP. The COHP, which is the Hamiltonian population weighted density of states (DOS), is identical with the crystal orbital overlap population.

II. Results and Discussion

Twenty four potentially applicable structure types have been used as inputs in the structural optimization calculations for the $MBeH_3$ compounds (Pearson structure classification notation in parenthesis): $KMnF_3$ (*tP*20), $GdFeO_3$ [$NaCoF_3$ (*oP*20)], $KCuF_3$ (*tI*20), $BaTiO_3$ [$RbNiF_3$ (*hP*30)], $CsCoF_3$ (*hR*45), $CaTiO_3$ [$CsHgF_3$ (*cP*5)], PCF_3 (*tP*40), $KCuF_3$ (*tP*5), $KCaF_3$ (*mP*40), $NaCuF_3$ (*aP*20), $SnTlF_3$ (*mC*80), $KCaF_3$ (*mB*40), $LiTaO_3$ (*hR*30), $KCuF_3$ (*oP*40), $PbGeS_3$ (*mP*20), $CaKF_3$ (*mP*20), $KNbO_3$ (*tP*5), $KNbO_3$ (*oA*10), $KNbO_3$ (*hR*5), $LaNiO_3$ (*hR*30), $CaTiO_3$ (*oC*10), $FeTiO_3$ (*hR*30), $SrZrO_3$ (*oC*40), $BaRuO_3$ (*hR*45), and α-$CsMgH_3$ (*Pmmm*).[21,22] From the above structural starting points, full geometry optimization has been carried out without any constrains on the atomic positions and unit-cell parameters.

Structural Features of $LiBeH_3$. In 1987 Overhauser[23] proposed the crystal structure of $LiBeH_3$ (space group $F\bar{4}3m$) by analyzing the X-ray powder diffraction data reported by Bell and Coates.[24] The author has also suggested that $LiBeH_3$ could have an electron density as high as that in metallic hydrogen and the material could accordingly be a high-temperature superconductor. A number of electronic−structure calculations have, in fact, already been performed on $LiBeH_3$,[25−29] using a variety of computational approximations. Most of these calculations conclude with insulating behavior and a large gap at the Fermi level (E_F). From the observed XRD pattern of Bell and Coates,[24] Selvam and Yvon recalculated the structure of $LiBeH_3$ and they commented that $LiBeH_3$ may form in $Fm\bar{3}m$ and concluded that high-quality diffraction data (preferably on single crystals) are required to find the accurate structure.[30] It should be noted that most of the alkali- or alkaline-earth-based hydrides are well-defined stoichiometric compounds and the hydrogen site occupancy in the matrix is always one. However, in $LiBeH_3$ phases, the reported H occupancy is almost 0.188 (six H atoms are distributed over 32 equivalent lattice sites), which is similar to the metal hydride systems. From this point of view, Selvam and Yvon have proposed that the experimentally established structure for $LiBeH_3$ may not be correct.[30]

Among the considered structures, $NaCoF_3$- and $NaCuF_3$-type derived atomic arrangements occur at the lowest total energy, and both phases (transformed into another phase) have exactly the same total energy. This type of situation sometimes arises when we do the full geometry optimization. Hence, we performed the symmetry analysis for the optimized data for both phases. Our symmetry analysis shows that during the structural relaxation processes the low-symmetry (triclinic) $NaCuF_3$ phase of $LiBeH_3$ transforms into the somewhat high-symmetry ($NaCoF_3$-type orthorhombic) phase. It is well known that the system sometimes, instead of relaxing to the local minimum, relaxes to the global minima as is the case here. The $LiBeH_3$ structure consists of corner-sharing BeH_6 octahedra (see Figure 1a). From the interatomic Be−H distances (varying from 1.604 to 1.632

(16) Perdew, J. P. *Electronic Structure of Solids*; Ziesche, P., Eschrig, H., Eds.; Akademie Verlag: Berlin, 1991. Perdew, J. P.; Burke, K.; Wang, Y. *Phys. Rev. B* **1996**, *54*, 16533. Perdew, J. P.; Burke, S.; Ernzerhof, M. *Phys. Rev. Lett.* **1996**, *77*, 3865.

(17) Blöchl, P. E. *Phys. Rev. B* **1994**, *50*, 17953. Kresse, G.; Joubert, J. *Phys. Rev. B* **1999**, *59*, 1758.

(18) Kresse, G.; Hafner, J. *Phys. Rev. B* **1993**. 47, R558. Kresse, G.; *Furthmuller J. Comput. Mater. Sci.***1996**, *6*, 15.

(19) Vajeeston, P.; Ravindran, P.; Kjekshus, A.; Fjellvåg, H. *Appl. Phys. Lett.* **2004**, *84*, 34.

(20) Krier, G.; Jepsen, O.; Burkhardt, A.; Andersen, O. K. *Tight Binding LMTO-ASA Program Version 4.7*; Stuttgart, Germany, 2000. Dronskowski, R.; Blöchl, P. E. *J. Phys. Chem.* **1993**, *97*, 8617.

(21) *Inorganic Crystal Structure Database*; Gmelin Institut: Germany, 2006/2.

(22) Renaudin, G.; Bertheville, B.; Yvon, K. *J. Alloys Compd.* **2003**, *353*, 175.

(23) Overhauser, A. W. *Phys. Rev. B* **1987**, *35*, 411.

(24) Bell, N. A.; Goates, G. E. *J. Chem. Soc. A* **1968**, *628*, 1968.

(25) Press, M. R.; Rao, B. K.; Jena, P. *Phys. Rev. B* **1988**, *38*, 2380.

(26) Seel, M.; Kunz, A. B.; Hill, S. *Phys. Rev. B* **1989**, *39*, 7949.

(27) Gupta, M.; Percheron-Guegan, A. P. *J. Phys. F* **1987**, *17*, L201.

(28) Yu, R.; Lam, P. K. *Phys. Rev. B* **1988**, *38*, 3567.

(29) Martins, J. L. *Phys. Rev. B* **1988**, *38*, 12776.

(30) Selvam, P.; Yvon, K. *Phys. Rev. B* **1989**, *39*, 12329.

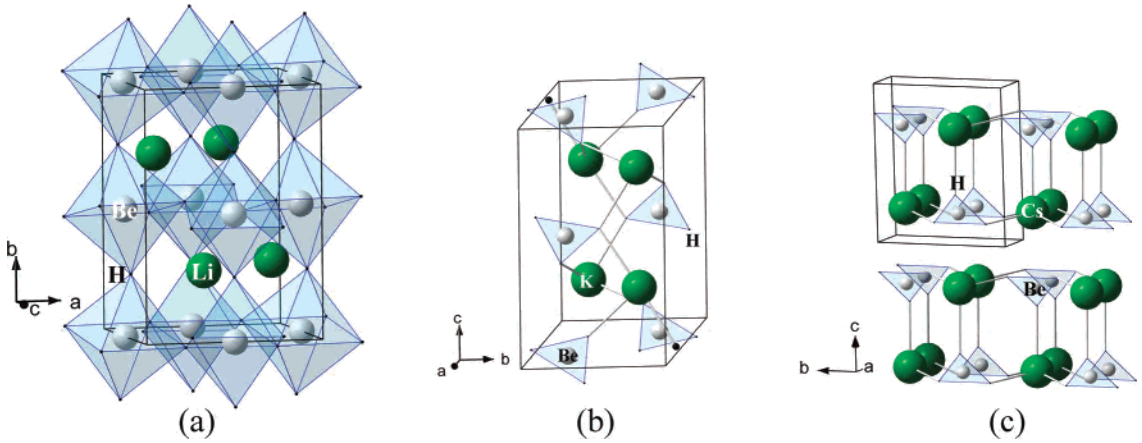

Figure 1. Predicted crystal structures of (a) $LiBeH_3$ ($NaCoF_3$; *Pnma*), (b) $KBeH_3$ and $RbBeH_3$ ($CaCO_3$(II); $P2_1/c$), and (c) $CsBeH_3$ ($KClO_3$; $P2_1/m1$).

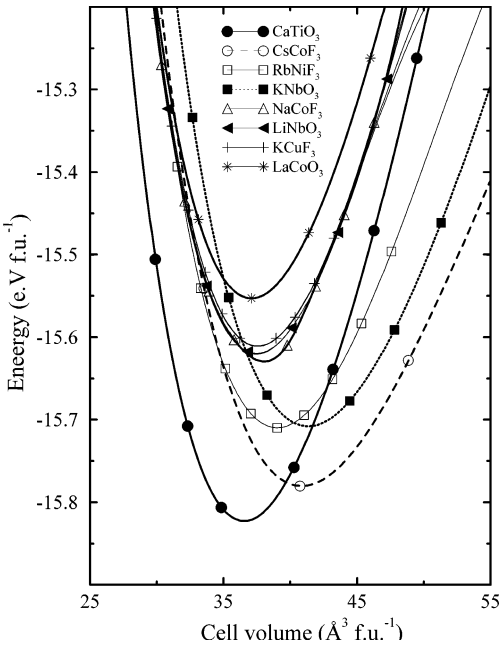

Figure 2. Cell volume vs total energy curves for $NaBeH_3$ in different possible structural arrangements (structure-type inputs are specified on the illustration). For clarity, only the eight variants with the lowest total energy are documented on the illustration.

Å) and H−Be−H angles (ranging between 89.3° and 90.7°), it is evident that the BeH_6 octahedra are slightly distorted. Li is surrounded by eight H atoms and the Li−H distances vary from 1.967 to 2.168 Å. The shortest H−H separation in the $LiBeH_3$ structure exceeds 2.301 Å and is consistent with the H−H separation found in other complex/metal hydrides.

Structural Features of $NaBeH_3$. According to the structural optimization calculations with the considered 24 structural inputs, the $CaTiO_3$-type variant (Figure 2) is found to have the lowest total energy. Similar to the $LiBeH_3$ phase, this $NaBeH_3$ structure also consists of corner-sharing ideal BeH_6 octahedra and the structure is an inverse perovskite-type structure (for a more detailed structural description, see ref 31). The present finding of stabilization of the inverse perovskite structure in the $NaBeH_3$ phase appears to emphasize the significance of size factors associated with both Na and Be cations. It should be noted that, in general, perovskites containing the Li^+ ion plus alkaline earth elements or Eu^{2+}, commonly adopt the inverse perovskite structure (eg. $BaLiF_3$, $BaLiH_3$, $EuLiH_3$, $SrLiH_3$[32−35]).

Structural Features of $KBeH_3$, $RbBeH_3$, and $CsBeH_3$. The results obtained from structural optimizations for the $KBeH_3$ and $RbBeH_3$ phases show that the $PbGeS_3$-type input structure proved to have the lowest total energy. However, the symmetry analysis for the optimized data gives the $CaCO_3$(II)-type structural arrangement, which was not included in the starting structures. Both $CaCO_3$(II) and $PbGeS_3$ phases have monoclinic structures with *P*121/*c* symmetry. However, the only main difference between these structures is that the former one consists of almost-planar CO_3 molecules in the Ca matrix and the later has ideal GeS_4 tetrahedral arrangement in the Pb matrix.

Similarly for the $CsBeH_3$ phase, the $PbGeS_3$-type structural input was found to have the lowest total energy and the symmetry analyses gave a $KClO_3$-type structure as the final structure. Both $CaCO_3$(II) and $KClO_3$ structure types are monoclinic, and the atomic arrangements also have close similarity (see Figure 1c). These structures consist of almost-separated BeH_3 planar molecules and are linked by alkali atoms. This structural feature is entirely different from that of the known compounds in the ABH_3 family.[36−40] All three phases have an almost similar Be−H distance (around 1.4 Å), which is much smaller than that in $LiBeH_3$ and $NaBeH_3$. Similarly, the H−H separation in these compounds is ∼2.4 Å. Some of these phases have interesting high-pressure

(31) Vajeeston, P.; Ravindran, P.; Fjellvåg, H. *J. Alloys Compd.* **2007** doi: 10.1016/j.jallcom.2006.12.058
(32) Boumriche, A.; Gesland, G. Y.; Bolon, A.; Rousseau, M. *Solid State Commun.* **1994**, *91*, 125.
(33) Messer, C. E.; Hardcastle, K. A. *Inorg. Chem.* **1964**, *3*, 1327.
(34) Messer, C. E.; Eastman, J. C.; Mers, R. G.; Maerland, A. *J. Inorg. Chem.* **1964**, *3*, 776.
(35) Orgaz, E.; Gupta, M. *J. Alloys Compd.* **1995**, *231*, 147.
(36) Rönnebro, E.; Noréus, D.; Kadir, K.; Reiser, A.; Bogdanovic, B. *J. Alloys Compd.* **2000**, *299*, 101.
(37) Bertheville, B.; Fischer, P.; Yvon, K. *J. Alloys Compd.* **2002**, 330−332, 152.
(38) Gingl, F.; Vogt, T.; Akiba, E.; Yvon, K. *J. Alloys Compd.* **1999**, *282*, 125.
(39) Bastide, J. P.; Bouamrane, A.; Claudy, P.; Letoffe, J.-M. *J. Less-Common Met.* **1987**, *136*, L1.
(40) Geller, S. *J. Chem. Phys.* **1956**, *24*, 1236.

Table 1. Optimized Equilibrium Structural Parameters, Bulk Modulus (B_0), and Pressure Derivative of Bulk Modulus (B_0') for the $MBeH_3$ (M = Li, K, Rb, Cs) Series

compound (space group; Pearson symbol)	unit cell (Å)	positional parameters	B_0 (GPa)	B_0'
$LiBeH_3$ (*Pnma*; *aP*20)	$a = 4.5361$	Li(4c) : 0.4500, 3/4, 0.4897	63.1	3.5
	$b = 6.2992$	Be(4b) : 0.0, 0.0, 1/2		
	$c = 4.4104$	H1(4c) : 0.9835, 1/4, 0.4305		
		H2(8d) : 0.7083, 0.9644, 0.2895		
α-$KBeH_3$ ($P2_1/c$; *aP*20)	$a = 7.0850$	K(4e) : 0.76352, 0.7448, 0.7832	10.9	5.2
	$b = 5.5621$	Be(4e) : 0.7492, 0.2534, 0.0021		
	$c = 8.9483$	H1(4e) : 0.6158, 0.3263, 0.8605		
	$\beta = 107.45$	H2(4e) : 0.8609, 0.4262, 0.1037		
		H3(4e) : 0.7832, 0.0100, 0.0362		
$RbBeH_3$ ($P2_1/c$; *aP*20)	$a = 7.4390$	Rb(4e) : 0.7576, 0.7458, 0.7705	10.5	4.87
	$b = 5.7899$	Be(4e) : 0.73874, 0.2521, 0.00477		
	$c = 9.4579$	H1(4e) : 0.6162, 0.3583, 0.8779		
	$\beta = 108.05$	H2(4e) : 0.8604, 0.3885, 0.1172		
		H3(4e) : 0.7476, 0.0101, 0.0159		
$CsBeH_3$ ($P2_1/m1$; *aP*20)	$a = 5.0969$	Cs(2e) : 0.8178, 3/4, 0.2310	8.6	5.1
	$b = 5.9359$	Be(2e) : 0.2390, 1/4, 0.2386		
	$c = 7.8451$	H1(2e) : 0.0930, 1/4, 0.3608		
	$\beta = 107.97$	H2(4f) : 0.3031, 0.4513, 0.1724		

behavior, and the results will be published in a forthcoming article along with that for the $AMgH_3$ series.

Although these compounds have isoelectronic configurations for all involved components, they stabilize in rather different crystal structures. The broad features of the structural arrangement vary from Li to K along the series from orthorhombic−cubic−monoclinic. Generally the variation in the crystal structures of ABX_3 compounds can be rationalized in terms of the Goldschmidt tolerance factor (t). The t factor for the perovskite-like compounds ABX_3 is defined as $t = (R_X + R_A)/\sqrt{2}(R_X + R_B)$ where R_A, R_B, and R_X refer the ionic radii[41] of the elements A, B, and X, respectively. For the six coordinated H^- ions, we have used 1.4 Å as ionic radii, as used in ref 22. For the three coordinated H^- ions, there is no tabulated value available for the t calculation. Hence, we have used the calculated Be−H distances for finding the ionic radii of three coordinated H^- ions, and the corresponding calculated value is 1.24 Å. The value of t may be used as an indicator of the tendency for structural transitions and for specification of the deformation in the octahedral coordination at the B site in a given perovskite family member.[22,42] For cubic arrangement, t should be in the range 0.89−1.00; the range 0.8−0.89 should be indicative of tetragonal or orthorhombic distortion of the cubic symmetry, and t above 1 should single out hexagonal (trigonal) stacking variants of the perovskite family. The t values for the compounds under investigation vary from 0.89 to 1.49 [0.89 ($LiBeH_3$), 1.08 ($NaBeH_3$), 1.35 ($KBeH_3$), 1.42 ($KBeH_3$), and 1.49 ($CsBeH_3$)]. Consistent with the Goldschmidt empirical rule, t takes a value close to 1 for cubic $NaBeH_3$, and this undistorted perovskite arrangement contains perfect octahedra. For the case with t less than 1 (viz. M = Li) there occurs distorted octahedra. In the case of $KBeH_3$, $RbBeH_3$, and $CsBeH_3$, the ground-state structures deviate from a perovskite-like framework.

Vinet et al.[43] have proposed an universal equation of state (UEO) which will be valid for all classes of solids under compression. According to them, if one defines x as $(V/V_0)^{1/3}$ and $H(x) = x^2P(x)/3(1 - x)$, then the $\ln[H(x)]$ versus $1 - x$ curve should be nearly linear and obey the relation$\ln[H(x)] \approx \ln(B_0) + \eta(1 - x)$. The isothermal EOS is expressed as $P = [3B_0(1 - x)/x^2] \exp[\eta(1 - x)]$. The slope of the curve (η) is related to the pressure derivative of the bulk modulus (B_0') by $\eta = (3/2)[B_0' - 1]$.

By fitting the total energy as a function of cell volume using the UEO, the bulk modulus (B_0) and its pressure derivative (B_0') are obtained (Table 1), but no experimental data for comparison are yet available. The bulk modulus decreases monotonically when we move from Li to Cs, and its pressure derivative increases correspondingly. The variations in B_0 and B_0' are accordingly correlated with variations in the size of M and consequently also with the cell volume. Compared to intermetallic-based hydrides, these compounds have low B_0 values, implying that they are soft and easily compressible. The soft character of the $MBeH_3$ materials arises from a high degree of ionic character in the chemical bonding. Hence, one can expect that destabilization of some of the hydrogen atoms from the matrix may be feasible. However, the Be−H bonds are likely to be strong. Accordingly, the integrated crystal orbital Hamilton population (ICOHP) study on these phases shows that the Be−H interaction is much stronger than the other interactions. The calculated ICOHP values for Be−H along this series vary from 0.68 to 1.14 eV (following the sequence Li < Na < K < Rb < Cs). On the other hand, when we move from Li to Cs, the calculated ICOHP values for the M−H interactions decrease from 0.34 to 0.06 eV (following the sequence Cs < Rb < K < Na < Li). This may be the possible reason (due to the strong Be−H and Li−H/Na−H bonding interaction) why $LiBeH_3$ has a higher bulk modulus than the rest of the phases in this series. This finding suggests that one needs more energy to break the Be−H bond in order to remove the hydrogen from these phases. In fact, experience from other complex aluminum-containing hydrides shows that one needs high temperature to break Al−H bonds. From this point of view, one can expect these $MBeH_3$ phases also to release hydrogen at elevated temperature only. Hence, these materials may not be suitable for onboard transportation

(41) Shannon, R. D. *Acta Crystallogr., Sect. B* **1976**, *32*, 751.
(42) *Perovskites Modern and Ancient*; Mitchell, R. H., Ed.; Almaz: Thunder Bay, Canada, 2002.
(43) Vinet, P.; Rose, J. H.; Ferrante, J.; Smith, J. R. *J. Phys.: Condens. Matter* **1989**, *1*, 1941

Table 2. Calculated Hydride Formation Energy (ΔH; in kJ mol^{-1}) According to Eqs 1−4 for the $MBeH_3$ Series

compound	ΔH_1	ΔH_2	ΔH_3	ΔH_4
$LiBeH_3$	28.85	−58.89	8.74	−79.01
$NaBeH_3$	−0.200	−45.21	−20.37	−65.37
$KBeH_3$	−2.94	−45.59	−23.05	−65.70
$RbBeH_3$	−10.37	−45.36	−30.49	−65.48
$CsBeH_3$	−16.75	−53.85	−36.87	−73.96

Table 3. Calculated Bader Charges (BC) Are Given in Terms of e and Energy Band Gap (E_g in eV) for the $MBeH_3$ Series

compounds	atom	BC	E_g
$LiBeH_3$	Li	+0.87	2.26
	Be	+1.46	
	H	−0.79	
$NaBeH_3$	Na	+0.84	1.79
	Be	+1.45	
	H	−0.74	
$KBeH_3$	K	+0.84	3.44
	Be	+1.27	
	H	−0.71	
$RbBeH_3$	Rb	+0.84	3.27
	Be	+1.27	
	H	−0.71	
$CsBeH_3$	Cs	+0.84	3.22
	Be	+1.28	
	H	−0.71	

applications. However, additive substitution (particle size control) may reduce the decomposition temperature considerably, as it was observed in alanates. Further research is needed in this direction.

Formation-Energy Considerations. Formation enthalpy is the best aid to establish whether theoretically predicted phases are likely to be stable, and also such data may serve as guides for possible synthesis routes. In this study we have considered four possible reaction pathways (eqs 1−4) and estimated the associated formation enthalpy, as listed in Table 2. In general, synthesis of $MBeH_3$ compounds from an equiatomic MBe matrix is not possible, as the alkali metals and beryllium are immiscible in the solid and liquid state (except the Be_2K phase in the K−Be phase diagram).[44] Schumacher and Weiss[45] have suggested that the ternary $MMgH_3$ hydrides can be synthesized directly by a reaction between M and Mg in hydrogen atmosphere at elevated temperatures. A similar approach may also be valid for the $MBeH_3$ series. However, most of the $MMgH_3$ compounds have also been synthesized from the appropriate combination of binary hydrides.[36−39] This shows that, among the considered reaction pathways, paths 1 and 4 are experimentally verified whereas paths 2 and 3 are open for verification or rejections.

The results show that reaction pathways 1−4 give rise to an exothermic reaction for the $MBeH_3$ compounds (except for $LiBeH_3$). Hence, preparation of $LiBeH_3$ from LiH and BeH_2 (pathway 1) and LiH + Be + H_2 (pathway 3) are not likely to be successful. All $MBeH_3$ compounds are seen to exhibit high formation energies according to pathway 4. Hence, for all the studied phases, pathway 4 is clearly the energetically most favorable, and we suggest that it should

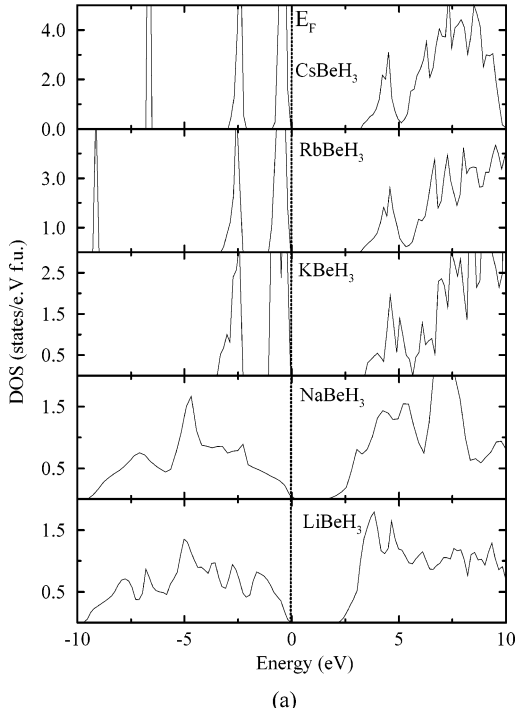

(a)

Figure 3. Calculated total density of states for $MBeH_3$. The Fermi level is set at zero energy and marked by the vertical dotted line.

be possible to synthesize/stabilize these compounds using this preparatory route. However, it should be noted that the kinetic aspects of these reaction pathways are not considered in the present calculation and may change this picture. Hence, further investigations are needed in this direction.

Chemical Bonding. In previous studies[15,46,47] on hydrides we have demonstrated that several theoretical tools are needed in order to draw more assured conclusions regarding the nature of the chemical bonding. In $MMgH_3$ series we found[15] that all the phases are basically saline hydrides similar to the parent alkali-/alkaline-earth mono-/dihydrides. Generally one may expect that these $MBeH_3$ series may also have almost similar bonding behavior.

The total DOSs at the equilibrium volumes for the ground-state structures of the $MBeH_3$ compounds are displayed in Figure 3, and site-projected DOSs for $LiBeH_3$ and $CsBeH_3$ are shown in Figure 4. All $MBeH_3$ compounds have a finite energy gap (E_g varying between 1.8 and 3.3 eV) between the valence band (VB) and the conduction band (CB), and hence, these phases can be considered as insulators. It is commonly recognized that theoretically calculated energy gaps for semiconductors and insulators are strongly dependent on the approximations used and, in particular, on the exchange and correlation terms of the potential. In general, the band gaps obtained from the density functional calculations always underestimate the experimental band gap. According to textbook chemistry, the insulating behavior of these materials can be explained as follows. Each formula unit, one electron from M fill one of the three originally

(44) *Binary Alloy Phase Diagrams*, 2nd ed.; ASM International: Washington, DC, 1990.
(45) Schumacher, R.; Weiss, A. *J. Less-Common Met.* **1990**, *163*, 179.
(46) Ravindran, P.; Vajeeston, P.; Vidya, R.; Kjekshus, A.; Fjellvåg, H. *Phys. Rev. Lett.* **2002**, *89*, 106403.
(47) Vajeeston, P.; Ravindran, P.; Kjekshus, A.; Fjellvåg, H. *Phys. Rev. B* **2005**, *71*, 216102.

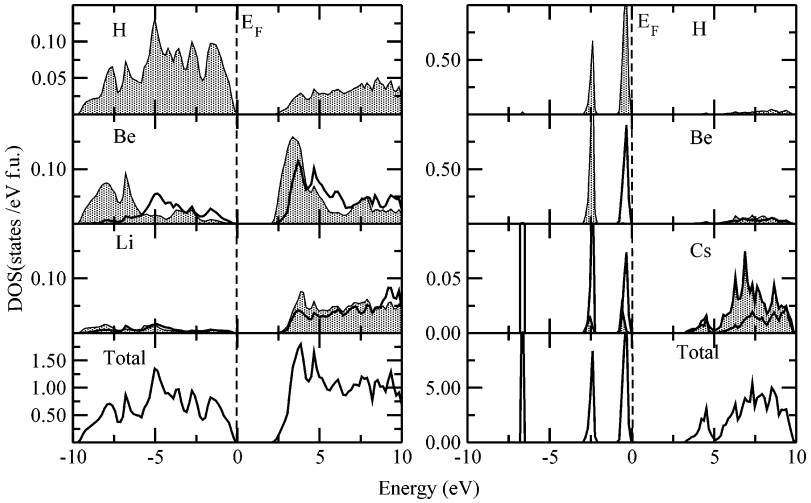

Figure 4. Calculated partial DOS for $LiBeH_3$ and $CsBeH_3$ phases. The Fermi level is set at zero energy and marked by the vertical dotted line; s states are shaded.

half-filled H s orbitals and the other two are filled by electrons from Be, resulting in a complete filling of the VB and accordingly an insulating behavior. The complex hydrides $MAlH_5$ (M = Mg, Ba),[48] M_3AlH_6 (M = Li, Na, K),[49,50] and MAH_4 (A = B, Al,Ga)[12,51] also exhibit similar insulating behavior. This suggests that one can generally expect wide band gap in complex hydrides with octahedral/tetrahedral coordinated structural units. On moving from $LiBeH_3$ to $CsBeH_3$, owing to the enlargement of the interatomic distances, the calculated width of VB decreases from 9.62 to 3.28 eV. In both $LiBeH_3$ and $NaBeH_3$, the VB region becomes single, and when one move to $KBeH_3$, $RbBeH_3$, and $CsBeH_3$, it becomes split into two regions and the bottom-most region belongs to semicore K 3p (in $KBeH_3$ this region is present at −12 eV which was not shown in Figure 2), Rb 4p, and Cs 5p states, respectively. This may be due to the variation in the coordination number for Be along this series. The 2.5 eV energy region is mainly originated from Be s with considerable contribution from H s states. The similarity in shape and degenerate nature of the DOS distribution from Be s and H s states indicate the presence of hybridization interaction between these atoms. The region near E_F originates from H s, Cs s, and Be p states.

In order to elucidate the bonding situation more properly, we have calculated the partial density of states (PDOS) for $MBeH_3$. Owing to close similarity between the PDOS for $LiBeH_3$ and $NaBeH_3$, we have only shown the PDOS for $LiBeH_3$ in Figure 1. As seen from this illustration, the PDOSs for Li show very small contributions at the VB. At the Be site, also the amount of valence electron present is much smaller than that in neutral atom and this demonstrates that valence electrons are transferred from the Li and Be sites to the H sites. The Be s and p states are energetically degenerate almost in the whole valence band region. The considerably broad and energetically degenerate nature of Be s and H s states indicate noticeable hybridization interaction between Be and H. We have observed drastic changes in the valence band feature on going from $LiBeH_3$ and $NaBeH_3$ to the $KBeH_3$, $RbBeH_3$, and $CsBeH_3$ cases. As the latter phases have close similarity, we displayed PDOS of $CsBeH_3$ only. From Figure 1, one can see that in Li- and Na-based system the Be atoms are coordinated by hydrogen octahedrally, whereas in K-, Rb-, and Cs-based hydrides the coordination of Be by hydrogen is planar. This could be the reason for the drastic change in the valence band feature. In all phases, Be p and H s states are present in the vicinity of the Fermi level. Unlike $LiBeH_3$ and $NaBeH_3$, in $KBeH_3$, $RbBeH_3$, and $CsBeH_3$, the Be s and p states are well separated.

In order to gain further understanding about the bonding situation in $MBeH_3$ compounds, we turn our attention to charge-density, and electron-localization-function (ELF) plots. Again, the different members of the series exhibit similar features, and in view of that, we have only documented such plots for $NaBeH_3$ in Figure 5. According to the charge-density distribution at the Na, Be, and H sites, it is evident that the highest charge density resides in the immediate vicinity of the nuclei. As also evidenced from the almost spherical charge distribution, the bonding between Na and H is virtually purely ionic and that between Be and H is predominantly ionic with small directional character. The nature of charge distribution seen in Figure 5 appears to be typical for ionic compounds.[13] The main distinction between the bonding in $MBeH_3$ series and the situation in the $MAlH_4$ and M_3AlH_6 series is that the interaction between Be and H has more ionic character than that between Al and H.[47] The electron population between Na and the BeH_6 units is almost zero (viz. charges are depleted from this region), which reconfirms that the interaction between Na and BeH_6 units is virtually pure ionic.

(48) Klaveness, A.; Vajeeston, P.; Ravindran, P.; Fjellvåg, H.; Kjekshus, A. *Phys. Rev. B* **2006**, *73*, 094122.
(49) Vajeeston, P.; Ravindran, P.; Kjekshus, A.; Fjellvåg, H. *Phys. Rev. B* **2004**, *69*, 020104(R).
(50) Vajeeston, P.; Ravindran, P.; Kjekshus, A.; Fjellvåg, H. *Phys. Rev. B* **2005**, *71*, 092103.
(51) Vajeeston, P.; Ravindran, P.; Kjekshus, A.; Fjellvåg, H. *J. Alloys Compd*. **2005**, *387*, 97.

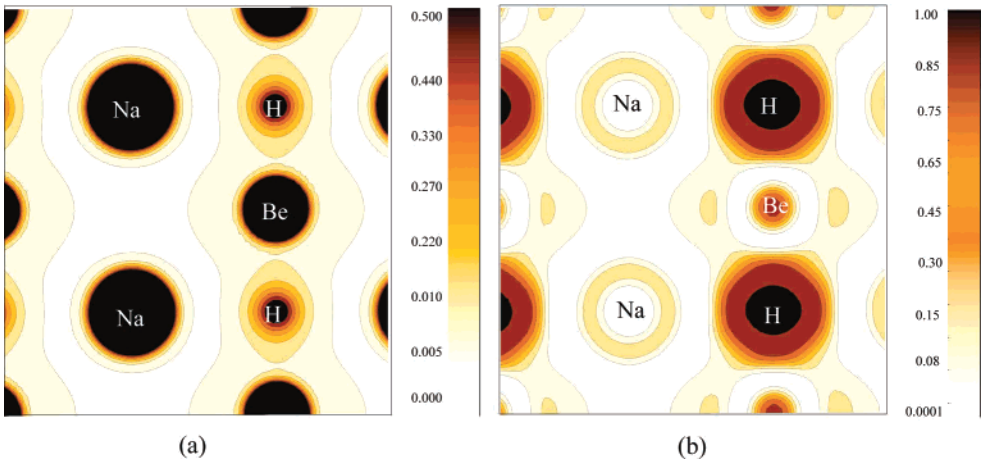

Figure 5. (Color online) Calculated plots of (a) valence-electron-charge density and (b) ELF for $NaBeH_3$. The illustrations refer to the (110) plane.

The calculated ELF plot (Figure 5b; for more information about ELF see refs 52−54) shows a predominant maximum of ca. 1 at the H site and these electrons have a paired character. The ELF values at the Na and Be sites are very low. The inference from this observation is that charges are transferred from the inhabitants of these sites to the H sites and there are certainly very few paired valence electrons left at the Na and Be sites. A certain polarized character is found in the ELF distribution at the H sites in all the complex hydrides we have investigated earlier.[47] The ELF distribution is, in contrast, quite isotropic in $MBeH_3$ and $MMgH_3$.[15] This provides another indication for a higher degree of ionic character in $MBeH_3$ series than in $MAlH_4$ and M_3AlH_6 series.

In an effort to quantify the bonding and estimate the amount of electrons on and between the participating atoms, we have done a Bader topological analysis. Although there is no unique definition to identify how many electrons are associated with an atom in a molecule or an atomic grouping in a solid, it has nevertheless proved useful in many cases to perform a Bader analysis.[55−57] In the Bader charge (BC) analysis, each atom of a compound is surrounded by a surface (called Bader regions) that run through minima of the charge density and total charge of an atom is determined by integration within the Bader region. The calculated BC for the $MBeH_3$ series are given in Table 2. The BC for M and H in the $MBeH_3$ compounds indicates that the interaction between M and BeH_6/BeH_3 is ionic (in all cases around one electron transferred from M to BeH_6/BeH_3). This finding is consistent with the DOS and charge density analyses. Within the BeH_6 and BeH_3 units, Be consistently donates nearly 1.5 (in $LiBeH_3$, and $NaBeH_3$) and 1.3 (in $KBeH_3$, $RbBeH_3$, and $CsBeH_3$) electrons to the H sites, respectively, which is much smaller than in the pure ionic picture. This is partly associated with the small covalency present between Be and H and also may be due to the artifact of Bader's "atom in molecule'' approach in making the boundaries to integrate charges in each atomic basin. However, consistent with the charge and DOS analyses, the BC always qualitatively shows that M and Be atoms donate electrons to the H site.

III. Conclusion

The crystal and electronic structures of the $MBeH_3$ (M = Li, Na, K, Rb, Cs) series have been studied by state-of-the-art density functional calculations. The ground-state crystal structures have been predicted from structural optimization of a number of structures using force as well as stress minimizations. The predicted crystal structure of $LiBeH_3$ to be $NaCoF_3$-type, $NaBeH_3$ to be $CaTiO_3$-type, $KBeH_3$ and $RbBeH_3$ to be $CaCO_3$ (II)-type, and $CsBeH_3$ to be $KClO_3$-type. Formation energies for the $MBeH_3$ series are calculated for different possible reaction pathways. For all these phases we propose that synthesis from elemental M and Be in hydrogen atmosphere should be a more feasible route. The $MBeH_3$ compounds are wide-band gap insulators and the insulating behavior is associated with well-localized, paired s-electron configuration at the H site. The chemical bonding character of these compounds is highly ionic according to analyses of DOS, charge density, ELF, and Bader charges. Our calculations suggest that all these compounds are energetically feasible to form and the thermodynamic and kinetic aspects of these materials for hydrogen-storage applications need further investigations.

Acknowledgment. The authors gratefully acknowledge the Research Council of Norway for financial support and R. Vidya and S. Zh. Karazhanov for fruitful discussions.

IC7015897

(52) Savin, A.; Becke, A. D.; Flad, J.; Nesper, R.; Preuss, H.; von Schnering, H. G. *Angew. Chem., Int. Ed. Engl.* **1991**, *30*, 409. Savin, A.; Jepsen, O.; Flad, J.; Andersen, O. K.; Preuss, H.; von Schnering, H. G. *Angew. Chem., Int. Ed. Engl.* **1992**, *31*, 187.
(53) Silvi, B.; Savin, A. *Nature* **1994**, *371*, 683.
(54) Becke, A. D.; Edgecombe, K. E. *J. Chem. Phys.* **1990**, *92*, 5397.
(55) Bader, R. F. W. *Atoms in molecules: A Quantum Theory*; Oxford University Press: New York, 1990.
(56) Henkelman, G.; Arnaldsson, A.; Jonsson, H. *Comput. Mater. Sci.* **2006**, *36*, 354.
(57) Guerra, C. F.; Handgraaf, J.-W.; Baerends, E. J.; Bickelhaupt, F. M. *J. Comput. Chem.* **2003**, *25*, 189.